COBEM 2023 27TH INTERNATIONAL CONGRESS OF MECHANICAL ENGENEERING

ABCM Brazilian Society of Mechanical Sciences and Engineering
27th ABCM International Congress of Mechanical Engineering
December 04-08, 2023, Florianópolis-SC, Brazil

COB-2023-1712
EXPERIMENTAL INVESTIGATION OF EMULSION FLOW AT PORE SCALE IN FRACTURED POROUS MEDIA

Alandmara Rosa Dionizio Leôncio
Ranena Verónica Ponce Flores
Marcio da Silveira Carvalho
Mechanical Engineering Department, Pontifícia Universidade Católica do Rio de Janeiro, RJ 22451-900, Brazil
adionizio@lmmp.mec.puc-rio.br; poncerv@puc-rio.br; msc@lmmp.mec.puc-rio.br

Sibani Lisa Biswal
Chemical and Biomolecular Engineering Department, Rice University, TX 77005-1827, United States
biswal@rice.edu

Abstract. *The high complexity and disparities between the matrix and fracture permeabilities of Naturally Fractured Reservoirs (NFR) lead to a rapid oil production decline. Emulsion flooding is a proved effective Enhanced Oil Recovery (EOR) technique, that can recover over 15% of the remaining oil when compared to water flooding. Emulsion droplets act as a mobility control agent blocking already swept water paths, reducing viscous fingering and therefore improving oil recovery. In this work we studied emulsion flow in NFR at pore scale through a microfluidic device designed with a central fracture flanked by high and low permeability zones. Evaluation of the flow of stable designed O/W emulsion at different capillary numbers (Ca) though injectivity tests and oil displacement by Water-Alternated-Emulsion (WAE) experiments showed the water mobility control exerted by the emulsion droplets through permeability reduction of the fractured models as a function of Ca. Moderated damage and significant pressure oscillation observed were linked to emulsion droplets blockage and percolation. In the injectivity tests, as Ca increases emulsion droplets undergo snap-off and move from the high permeability regions towards the low permeability zone. Impact of Ca in the emulsion blockage efficiency and in oil recovery was also observed in WAE tests.*

Keywords: *Naturally Fractured Reservoirs, Oil-in-Water Emulsions, Injectivity Tests, Oil Displacement Tests, Enhanced Oil Recovery.*

1. INTRODUCTION

Naturally Fractured Reservoirs (NFR) present high complexity and heterogeneity due to the coexistence of matrix and fracture, two porous media with distinct characteristics. Reservoir fractures have a relevant influence on fluid flow performance and oil recovery efficiency, which can make the assessment of fracture properties of great relevance (Allan and Sun, 2003). Depending on fracture penetration and orientation, fractured porous media can have fracture/matrix permeability contrast ratios of 1000 or more (Conn *et al.*, 2014). Due to this relationship, the fracture can provide very early breakthrough to the injected fluids due to the preferential flow paths in its network, while the matrix, with much lower porosity and permeability, provides oil storage and a rapid decline in oil production, which is unfeasible for the oil industry (Li and Firoozabadi, 2000; Camargo *et al.*, 2019). Therefore, there is particular interest in the interaction between fractures and the matrix in heterogeneous systems, and this challenge corroborates to updating the various conformance control techniques applied to reduce water channeling through high permeability channels or fractures.

Emulsion injection as a chemical Enhanced oil recovery (cEOR) method has shown improved sweep efficiency and additional oil recovery in several laboratory and field-scale experiments. It has been a promising candidate as a mobility control in capillary displacement tests at both micro and Darcy scales, based on many laboratory and pilot tests. Blocking caused by the emulsion is achieved by trapping the dispersed phase in the pore throats as they flow through the porous medium. As the droplets flow through the constrictions, an extra pressure gradient is needed to overcome the capillary resistance. More than 15% of the remaining oil can be recovered by emulsion flooding compared to just water flooding according to homogeneous Sandpack flooding tests (Mandal *et al.*, 2010). According to emulsion injection studies, additional oil recovery can be achieved due to several reasons such as reduced interfacial tension (IFT), modification of oil and water mobility, modification of rock wettability and permeability (Alvarado *et al.*, 2014) and flow diversion to low permeability paths due to blockage of previously swept areas (Zhou *et al.*, 2019; Chen and Tao, 2005; Guillen *et al.*, 2012).

Based on McAuliffe *et al.* (1973) works, emulsion flooding can cause a reduction in core permeability during the

injection of crude O/W emulsions and it strongly depends on the emulsion droplet size to pore ratio. If this ratio is lower than 1, very small droplets can pass through the pore throat without blockage phenomena and, when this ratio is higher than 1, the droplets need to warp, leading to a Jamin effect (Wright, 1933). This means that at higher flow rates, the pressure drop becomes greater, causing more droplets to overcome capillary resistance and deform to pass through the pore constrictions. As McAuliffe *et al.* (1973), others authors have reported a greater reduction in permeability at low flow rates and have shown that emulsion injection is more effective at low pressure gradients (Yu *et al.*, 2018; Chen *et al.*, 2018). Emulsion injection can be effective in blocking fractured and high permeability regions if the droplets have a large enough droplet size to keep this ratio close to 1. This is a major challenge as the emulsion needs to be stable and the emulsions above 100 μm in diameter are thermodynamically unstable and can easily coalesce during an injection phase. It influences the emulsion performance in porous media since droplet breakup or coalescence can lead to changes in the drop size distribution (DSD), and the aggregation and/or coalescence of the droplets drop must be avoided. In short, some authors defend that to cause obstruction, the droplets need to be in the range of 50 to 150% of the pore throats.

Microfluidic devices made by PDMS, glass and other polymeric materials have been versatile tools extensively used to visualise multi-phase flow displacement at micro-scale and to study pore scaling mechanisms involved in enhanced oil recovery experiments (Conn *et al.*, 2014). These systems may allow real-time in situ observation of fluid flow in complex systems involving multi-phase injection into fractured pore geometries. Conn *et al.* (2014) performed foam flooding oil displacement tests on a heterogeneous microfluidic porous 2D model with stratified permeability regions and a central fracture. Additional oil was displaced and greater sweeping efficiency occured compared to water flooding. In addition, the visual analysis of the micromodel showed the permeability region where the oil was mobilized and how the injected fluids invaded each permeability zone of the micromodel.

Capillary number (Ca) is an important parameter for oil trapping studies to be considered when working with EOR experiments. It can be calculated by the ratio between the displacing fluid phase viscosity (μ) times interstitial velocity (v) and the phases interfacial tension (σ) and determines how strong the trapped oil stays in a porous medium. Viscous forces dominate the flow if Ca is high and the extra pressure needed to deform the droplet as it flows through the constriction is negligible. If Ca is small, the more important force is the capillary and a stronger mobility reduction can occur, since it is more difficult to deform the droplets when they pass through the constrictions. A model to describe this behavior at pore scale through a mobility reduction factor, f, was proposed by Cobos *et al.* (2009) and Guillen *et al.* (2012). f can be calculated by the ratio of the average pressure measured during continuous phase injection, Δp_c, to that of the emulsion flooding, Δp_e. When $f \sim 1$, it is not a function of Ca if the emulsion droplets are much smaller than the pore throats. If Ca is high, $f \to 1$. Furthermore, if the droplets are in the same order of the pore constriction in size or higher, f is strongly dependent on Ca number.

The purpose of this work was to study the flow of stable O/W emulsions, in single and two-phase flow, as mobility control agents in a flanked micromodel device at different Ca's. The goal of an emulsion injection strategy in a fractured media is to generate sufficiently large droplets that can create resistance to flow in regions of high permeability and fracture, and divert the injected fluids to adjacent regions of low permeability that harbor trapped oil. By combining microfluidic technology with optical microscopy and high-quality visualization, it was possible to provide detailed information about the fluids interactions at pore scale in an idealized NFR model. Emulsion stability was studied through bottle tests and by its DSD evolution. Experiments were carried out to estimate the emulsion injectivity in reservoirs with different values of Ca and oil displacement tests (WAE injection) were performed to quantify the additional oil recovery, proving the benefit of emulsion as a mobility control agent, and the impact of the fracture presence in the development of production in oilfields.

2. MATERIAL AND METHODS

2.1 Design and fabrication of the microfluidic device - 2D Linear Norland Optical Adhesive 81 (NOA) Micromodel

A pattern was designed using computer design software, AutoCAD©, and printed on a high-resolution transparency printer. By soft lithography procedure (Xia and Whitesides, 1998; McDonald and Whitesides, 2002), this pattern is then transferred to a photo-resist (Xia and Whitesides, 1998). Next, a polydimethylsiloxane (PDMS) mold mixed with the curing agent at 10:1 ratio is manufactured by molding to the pattern and curing it in an oven around 60°C overnight. An Norland optical adhesive 81 (NOA81), a thiol-ene crosslinking polymer, is then poured into the PDMS mold and cured under UV light. Then, a glass substrate is prepared with a small film of the NOA, also cured in UV light, and the two halves of the device are irreversibly bonded through oxygen plasma treatment by a Plasma cleaner. The NOA was chosen to manufacture the devices because it is more robust than traditional PDMS microfluidic devices, the epoxy structure is more resistant to swelling by many organic solvents, and the surface-wetting behavior of these devices is more stable than PDMS. Furthermore, the Young's modulus of PDMS is 2.5 MPa, while that of the optical adhesive is around 325 MPa, which is less prone to pressure induced deformation and channel failure (Vavra *et al.*, 2018). The pore network designed using AutoCAD© is shown in Figure 1.

According to the micromodel design, the distance between the low and high permeability region forms a fracture width of approximately 440 μm. The high and low permeability matrices have pore throats of approximately 102 and 34 μm, respectively, and the channel of the entire micromodel is about 60 μm deep, which guarantees a pore volume (P_v) of 0.017mm^3, also calculated by mass difference. Both regions of the matrix are formed by round grains arranged in a square lattice. The permeabilities are much higher than those found in the reservoir rock to allow fluids to be visualized on a scale that can distinguish the fluid phases in the narrow pore throats and also capture the overall behavior and interaction of all three permeability regions simultaneously. Two additional holes, as showed in Figure 1-(c), were drilled in the micromodel at the entrance and exit of the porous medium for pressure acquisition and fluid injection/production, and polyethylene tube was inserted and fixed with epoxy.

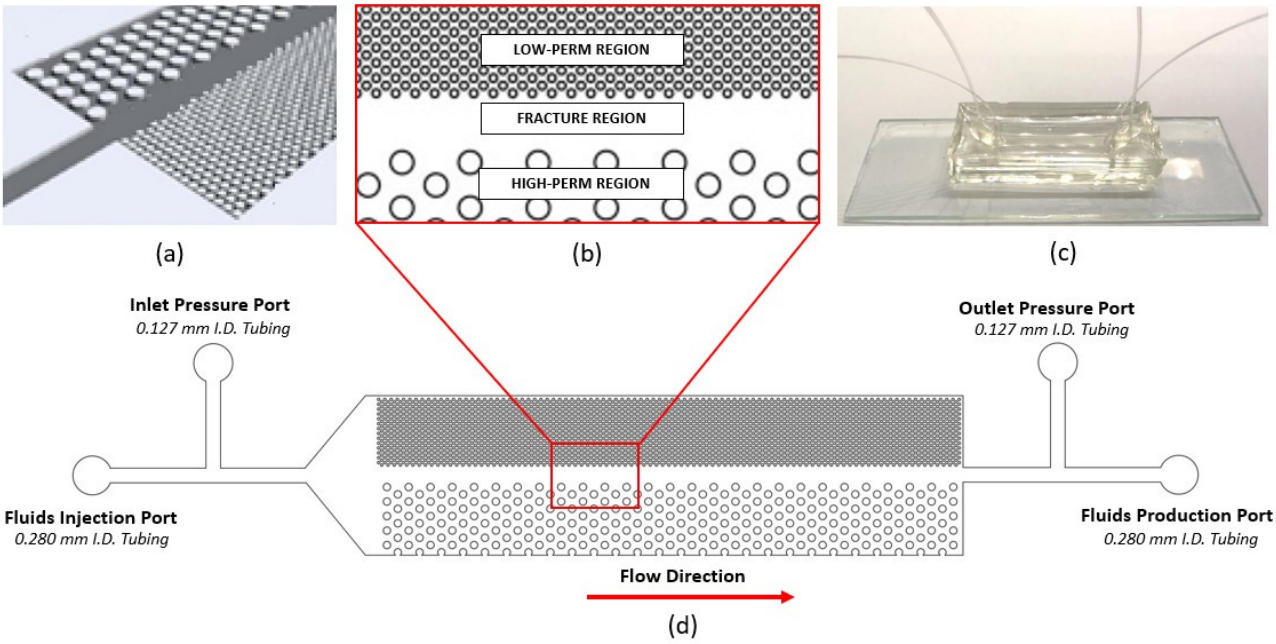

Figure 1. (a) 3D perspective cut of the CAD Photomask for NOA81 micromodel (b) Low, high and fracture regions of the micromodel (c) Real micromodel (d) 2D CAD Photomask evidencing inlet and outlet ports

2.2 Fluid Properties

All experiments were performed under ambient conditions of pressure and temperature (23°C) to minimize the complexity of the subject studied. The aqueous phase ($\mu = 1.03\ cP$) was prepared with the addition of 0.5% w/v of Bio-Soft N25-9 (Stepan) surfactant with (displacement tests) and without (injectivity tests) 0.5% Blue Dye in Milli-Q water. Bio-soft N25-9 is a high active nonionic surfactant based on a synthetic C12-15 linear alcohol ethoxylated with HLB 13.3. Developed by the Stepan Company, it is stable in acidic and alkaline aqueous solutions. Its critical micelle concentration (CMC) in Milli-Q water was measured in the value of 0.025 g/L using a Wilhelmy plate (DCAT 25©, Dataphysics Instruments). The emulsion dispersed phase and the oil used in the micromodel saturation step were composed of a light white paraffin mineral oil (VWR Chemicals BDH®, $\rho = 0.83\ g/cm^3$, and $\mu = 25\ cP$ at 20°C) with and without Oil Red dye at a concentration of 0.5% w/v, respectively. The oil-water IFT (σ) was around 4.26 mN/m, measured by a pendent drop technique. The function of dyeing fluids was to distinguish the aqueous phase, the oil used to saturate the micromodels and the emulsion injected in the analysis of microscopic images, since all were transparent fluids. In addition, all fluids used in the studied were previously filtered to eliminate impurities in the system.

2.3 Emulsion formation and stability

A stable O/W emulsion was formulated at an initial concentration of 1:1 phases ratio, in a total volume of 20 ml. To formulate a droplet-sized emulsion that could block both the fracture and the matrix micromodel regions, the goal was to find a formulation with d(0.5) and d(0.9) in the range of 50% to 150% of the low (34 μm) and high (102 μm) permeability pore throat, respectively, by chosen agitation method, time and speed to form an emulsion with an uniform appearance and without the presence of free water or oil at the end of the agitation. The emulsion was homogenized using a magnetic stirrer plate at 1150 RPM, for 10 minutes at 40°C. This method was applied due to the difficulty of obtaining emulsions with large droplets by conventional homogenizers equipments, such as an

Ultra Turrax mixer or a Sonication method. The temperature was necessary due to the difficulty in obtaining the desired emulsion size, as it modifies the viscosity of the fluids and improves the interaction of the surfactant with both phases, facilitating the formation of smaller droplets and a more stable emulsion. Initially, both phases were stirred for 30 minutes at 300 RPM and 40°C on a magnetic stirrer plate for uniform heating. With the aqueous phase in a 50 ml glass beaker at 1150 RPM, the oil was poured manually during the first 30 seconds of preparation. After 1 hour of rest, enough time for the emulsion to reach room temperature, the first microscopic analysis was performed to determine its DSD. The stability of the emulsion was studied by monitoring the formation of an oil film during a certain period of aging through bottle tests and analyzing the evolution over time of the DSD, obtained by an in-house developed Matlab© code routine that detects cycles on a microscope image and calculates the DSD-based number. To ensure a good representation of the total emulsion, approximately 40 images were collected for each analysis, ensuring a sample size of at least 1000 drops.

Figure 2 shows a microscopic image and the emulsion DSD, showing a wide size distribution that characterizes it as a polydisperse system. The graph shows the DSD as a curve of probability density function versus particle size, representing the density of a continuous random variable lying between a specific range of values. The D-values - statistical parameters of diameter measurements, including the median d (0.5) and d(0.9) that represent the diameters of which 50% and 90% of the droplet population have a diameter smaller than this value, respectively -, d(0.1), d(0.5), and d(0.9) on its first day (D1) were at least 26, 46, and 137 μm, respectively. According to the DSD curves, the emulsion was considerably stable without significant changes, through 5 consecutive days of stability studies, enough time to carry out the most long injection test. In terms of the constricted size distribution of the microfluidic device, droplets around 137 μm can flow with deformation or become trapped in the high permeability region by straining mechanism and smaller droplets can be captured by bridging mechanism. The efficiency of both capture mechanisms is strongly dependent on Ca.

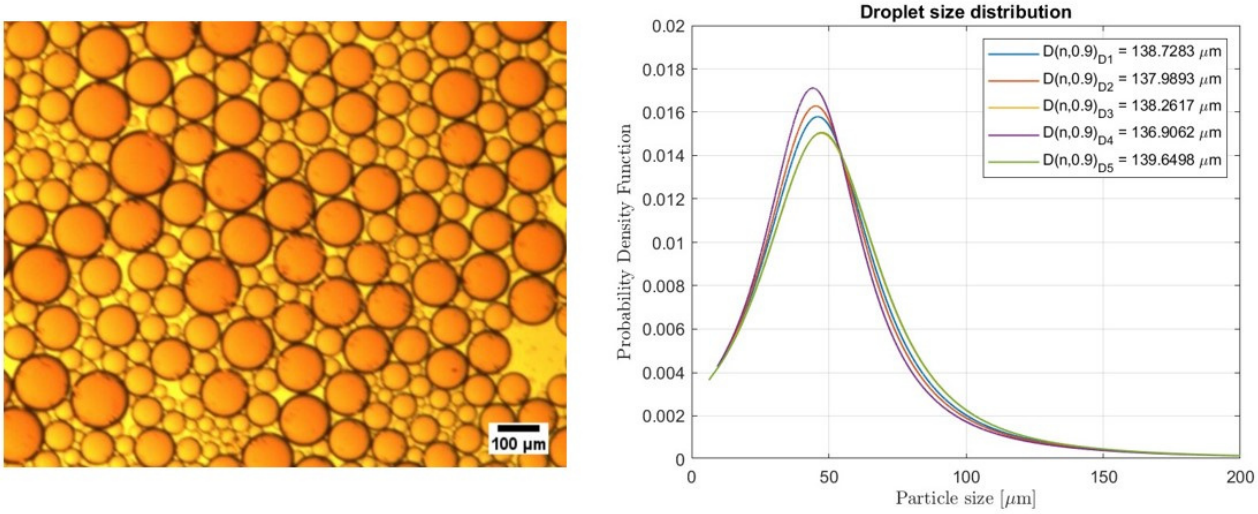

Figure 2. Microscopic image and Drop size distribuition of the emulsion system

2.4 Experimental procedures

Experimental setup: The micromodel and the pressure transducer were arranged in a support fitted to the base of the microscope, which allowed working with the micromodel inverted, to facilitate and have a better control of the emulsion injection. The injection system consisted of a syringe pump (KDS KD Scientific Model Legacy Dual Infusion Syringe), adapted to work with 3 syringes at the same time, for aqueous phase, oil phase, and emulsion injection. For the emulsion dilution procedure, 1 and 30 ml syringes were used for the emulsion and aqueous phases, respectively, to converge to an approximate dilution of 5/95 vol.%, this emulsion concentration was used in both, injectivity and WAE tests. A small I.D. tube (0.280 mm) was used for injection and production tubing to minimize gravitational segregation of the dispersed emulsion phase. Pressure data were computed every 0.1 second by a pressure transducer with a 0–20 psig diaphragm, Validyne P61 Differential Pressure Transmitter. The pressure tubing and transducer chambers were flushed with paraffin oil until air ceased to exit through the bleed valve screw holes and then sealed to prevent signal delay or fluid changes. And, to corroborate this, the pressure tapping tubing had a smaller I.D., 0.127 mm, than the fluids injection tubing. The fluids saturation and pressure drop across the microfluidic device were measured as a function of time and the injected micromodel P_v. All injection tests were performed in a system mounted on an Olympus IX81 microscope for detailed flow visualization and image acquisition. It was

obtained by acquiring live images at 10 frames per second and 2.5x magnification lens, with a resolution of 1920 x 1080 pixels, through an IMPERX CCD camera, designed for imaging applications that require high-quality images. Images were taken at different stages of the test to analyze the emulsion behavior and droplet capture mechanisms. Images of the entire micromodel were acquired by scanning the micromodel in the x directions and stitching all images together.

Image processing: The full images were treated in an in-house developed Matlab© code for equalization, pixel adjustment and quality enhancement, to ensure that all images have approximately the same error when calculating the fluid saturation. The saturation of the emulsion, oil and aqueous phase were determined using the ImageJ software, by treshhold technique and area analysis that allow to detect an image coverage area according to a color selected range.

Injectivity tests: Injectivity tests were performed to analyze the efficiency of emulsion flooding as a mobility control method during single-phase flow. It consisted of injecting the continuous emulsion phase (WF_1), followed by the emulsion (EMF), to compares the differential pressure response of both fluids, in a fixed Ca. Subsequently, a second continuous emulsion phase (WF_2) was performed to determine the permeability lost due to emulsion blockage, by calculating the Residual Resistance Factor (RRF) as the WF_1 to WF_2 pressure ratio. The WF_2 injection was made until reach the steady state on the injection pressure. This step by step was carried out at four Ca, namely $4.79E{-}06$, $9.59E{-}06$, $1.92E{-}05$ and $2.88E{-}05$, corresponding to flow rates from 0.1 to 0.6 ml/h, in order to plot the mobility reduction factor (f) curve to analyze the emulsion injection behavior. In all tests, 4 P_v of emulsion injection was performed after $\approx$ 10 P_v of WF_1, this injection scheme was kept the same during WAE tests.

WAE tests: Water-alternated-emulsion (WAE) injection is an alternative cEOR that can improve water mobility control and sweep efficiency through flow diversion. It consisted of injecting emulsion in between two batch of waterflooding. Based on the injectivity tests results, the flow rates of 0.05, 0.1, and 0.2 ml/h corresponding to Ca $2.39E{-}06$, $4.79E{-}06$ and $9.59E{-}06$ respectively, were selected for the microfluidic WAE tests. Prior to each experiment, CO_2 was injected for approximately 10 minutes to eliminate any trapped air in the pores, to ensure completely micromodel saturation. Then, Milli-Q was injected until completely saturating the micromodel. Milli-Q water without surfactant was used in this step to avoid oil emulsification during the oil saturation phase. Subsequently, it was displaced by the injection of 4 P_v of oil phase, enough to cease the water phase production, at the selected flow rate. At the end of this stage, images were acquired to determine S_{wi} and S_{oi}, the concentration of water and oil retained in the micromodel, after the steady state was reached, respectively. The subsequent steps were to carry out the first injection of 10 P_v of aqueous phase (WF_1), 1 P_v of diluted emulsion injection (EMF), and the second aqueous phase injection (WF_2), also in 10 P_v . Images were acquired after each step to determine the oil and water phases volume and emulsion droplets retained in the micromodel.

3. RESULTS

3.1 Injectivity test (single phase flow experiments)

The most important parameters for emulsion flooding, which can determine the efficiency of oil displacement in oilfield development, are the mobility reduction factor (f) and the residual resistance factor (RRF). The f of a given injectivity test is the mobility ratio of the aqueous phase (WF_1) to the emulsion (EMF) and reflects the ability to reduce mobility by emulsion flooding (Cobos *et al.* (2009); Guillen *et al.* (2012)). The RRF refers to the pressure ratio of the aqueous phase before (WF_1) and after (WF_2) the emulsion flows through the core and reflects the reduction in permeability or permeability damage caused by emulsion flooding. RRF values greater than 1 results in a better oil sweep efficiency. Higher RRF means more potential for improved oil sweep efficiency and greater additional oil recovery by emulsion flooding.

Table 1 summarizes the main parameters measured during all injectivity tests for each Ca evaluated, including their f and RRF, and the saturation of the emulsion dispersion phase trapped in the micromodel after WF_2. The processed images computed after WF_2 for each test follow in Figures 3, 4, 5, and 6. The emulsion saturation within the micromodel after the WF_2 injection is evidenced in processed microphotographs, for each Ca. f and RRF curves were plotted in Figure 7, evidencing a critical Ca for the study of $1.5E{-}05$ noted by a red line, determined as the Ca at which both curves begin to tend towards a constant behavior. It was noticed that droplets were trapped in the high permeability region only at Ca below $9.59E{-}06$ which according to f curve, is below the critical value where the emulsion droplet capture efficiency is increased,

It was observed during all tests, that while the emulsion flowed through the fracture region, the droplets diverted from the fracture to the low permeability region axially due to an extra pressure gradient caused by the emulsion flow in the fracture and in the high permeability region. This can be seen in Figure 3 and 4, where there are droplets trapped between the fracture and the low permeability interface, explained by a pressure gradient not high enough for them to percolate. At high Ca, due to the predominance of viscous forces, there were no droplets blocking the high permeability region. Instead, small oil ganglia from the emulsion remained trapped in the low-permeability

region. As the constrictions are so small, a huge pressure gradient would be required to mobilize them. The trapped column emulsion from Table 1 shows that the higher the Ca, the smaller the volume of the dispersed phase trapped due to this behavior. Another observation is that some droplets settled on the injection region in 1^{st} and 2^{nd} tests (Ca of $4.79E{-}06$ and $9.59E{-}06$), possibly due to this being a region of lower gradient pressure. Others created a preferential path along the path between the micromodel wall and the low permeability region. It is also possible to note a clogging mechanisms of straining and bridging in both testes. At higher Ca, the aqueous phase during WF_2 was able to mobilize a significant number of droplets, diverting them through the micromodel.

Figure 8 compares the differential pressure response of aqueous phase and emulsion injection for selected fixed flow rates. It is possible to observe an important increase in the differential pressure during the emulsion injection, in agreement to the results reported earlier by Cobos *et al.* (2009) and Guillen *et al.* (2012). The pressure curves during WF_2 in all tests stabilized at a level above WF_1, showing a reduction in permeability caused by the dispersed phase trapped in the pores and the aqueous phase mobility during the tests. As can be seen in the RRF curve, the lower the flow rate, the greater the RRF, that is, the greater the clogging of the porous medium by the emulsion drops, the same conclusion from the processed images. All results point to the same conclusion that the pore blocking efficiency drops with Ca increasing, so oil displacement tests were performed only at low Ca, below $9.59E{-}06$, values at which the droplets were trapped in the high permeability region.

Table 1. Injectivity tests parameters

Injectivity test	Ca	Δp_c [**WF$_1$**, psig]	Δp_e [**EMF**, psig]	Δp_c [**WF$_2$**, psig]	f	RRF	**Trapped emulsion** [%]
1^{st}	4.79 E-06	0.11	0.15	0.14	0.70	1.31	17.00
2^{nd}	9.59 E-06	0.30	0.36	0.34	0.83	1.15	13.90
3^{rd}	1.92 E-05	0.49	0.56	0.54	0.86	1.11	9.10
4^{th}	2.88 E-05	0.80	0.94	0.90	0.86	1.12	9.20

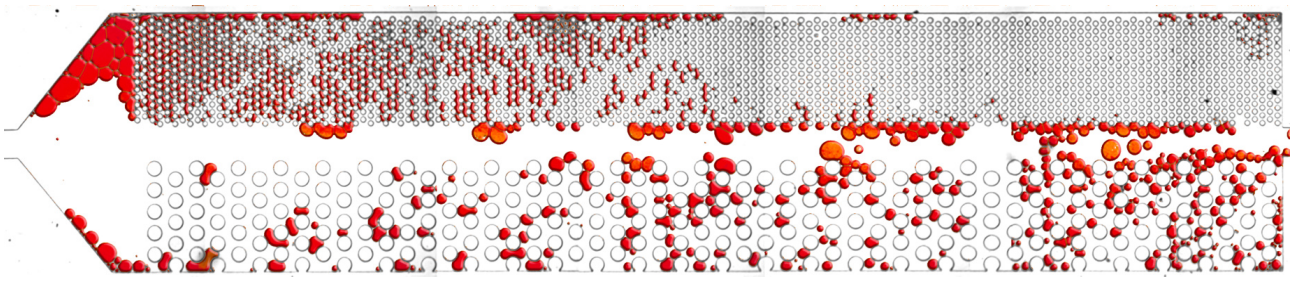

Figure 3. 2D X-Y cross section processed image of the micromodel of the 1^{st} Injectivity test after WF_2 ($Ca = 4.79E{-}06$). The aqueous phase and the background of the micromodel appear in white, and the emulsion droplets in red.

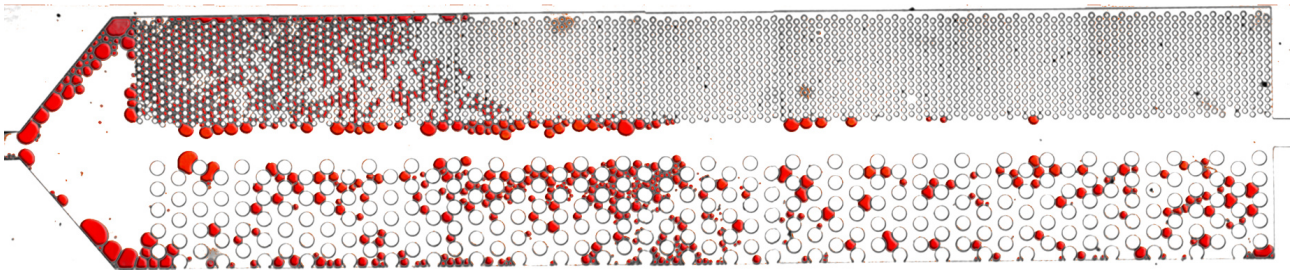

Figure 4. 2D X-Y cross section processed image of the micromodel of the 2^{nd} Injectivity test after WF_2 ($Ca = 9.59E{-}06$). The aqueous phase and the background of the micromodel appear in white, and the emulsion droplets in red.

3.2 WAE tests - Oil Displacement tests

Based on the results obtained in the injectivity tests, oil displacement tests were carried out working below the critical Ca determined by the f curve. The fixed Ca values adopted in the WAE tests were $2.39E{-}06$, $4.79E{-}06$, and

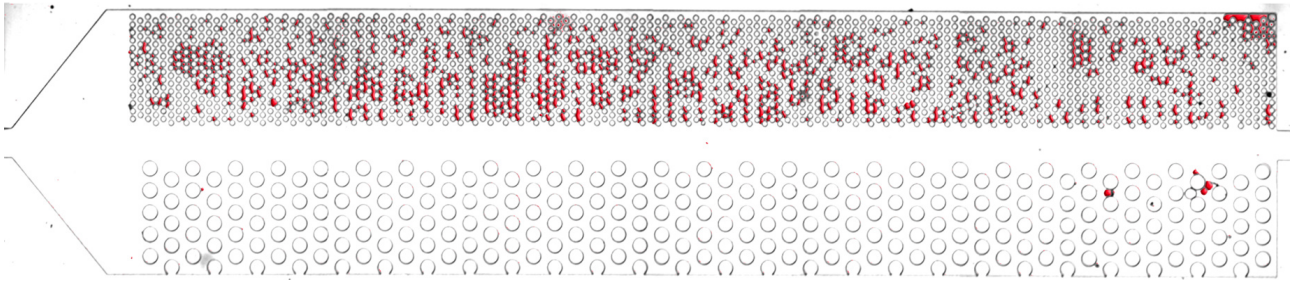

Figure 5. 2D X-Y cross section processed image of the micromodel of the 3^{rd} Injectivity test after WF_2 ($Ca = 1.92E{-}05$). The aqueous phase and the background of the micromodel appear in white, and the emulsion droplets in red.

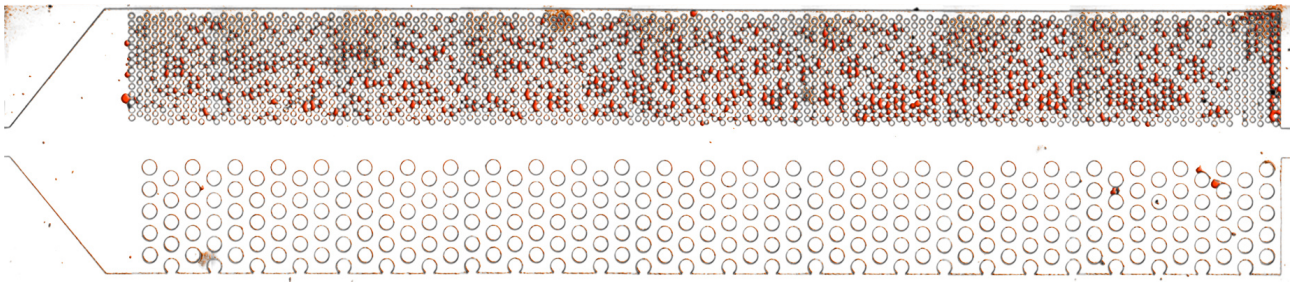

Figure 6. 2D X-Y cross section processed image of the micromodel of the 4^{th} Injectivity test after WF_2 ($Ca = 2.88E{-}05$). The aqueous phase and the background of the micromodel appear in white, and the emulsion droplets in red.

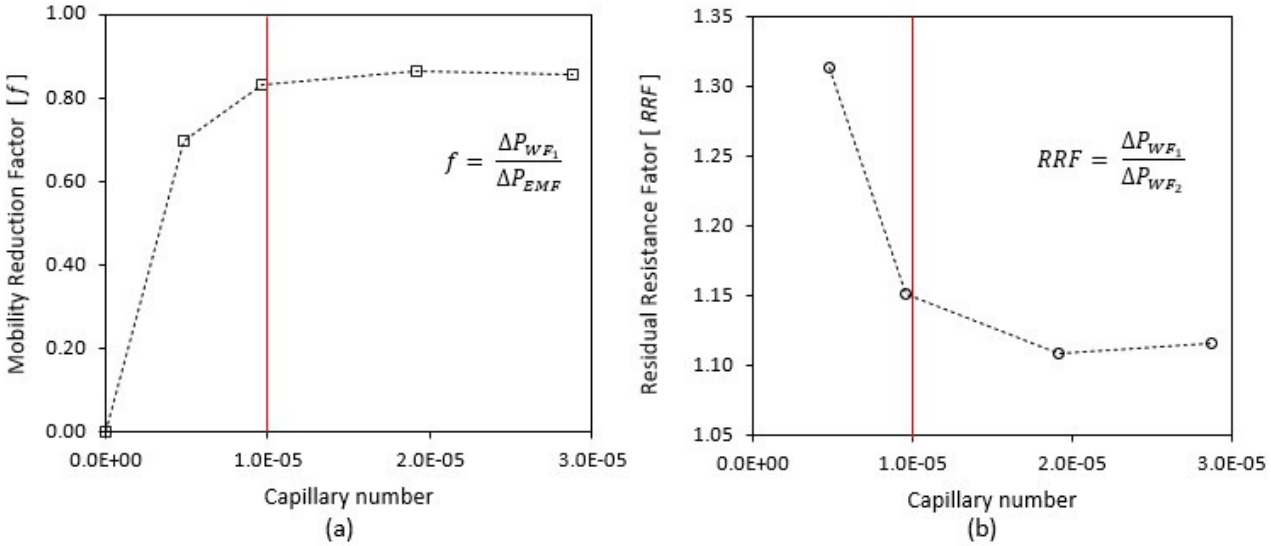

Figure 7. Effects of capillary number on (a) Mobility Reduction factor (f) and (b) Residual Resistence factor (RRF).

$9.59E{-}06$. Figures 9, 10, and 11 show the microscope processed images after WF_1 and WF_2 injection phases, where it is possible to notice the saturation of the oil and aqueous phases and of the emulsion present in the micromodel. Images were processed at each stage of each WAE test to determine the S_{wi}, S_{oi}, S_{or} and % of trapped emulsion after fluids injection along with the difference in residual oil saturation after both waterflooding processses. These parameters are displayed in Table 2, calculated from the image processing by ImageJ through the area analysis by color range, although only the most relevant images were displayed in this work related to emulsion effect visualization.

Analyzing the results shown in the Table 2, some expected results can be noted, such as high S_{or} values at low Ca after the WF_1. After the first water injection, the remaining oil saturation is high due to the very high viscosity ratio between the oil and aqueous phase. Also, the higher the Ca, the lower the S_{or} in the micromodel, because the pressure gradient generated in the porous medium during the injection is greater for high flow rates, facilitating the displacement of oil ganglia trapped in the pores. In this way, each test was carried out from a different initial state

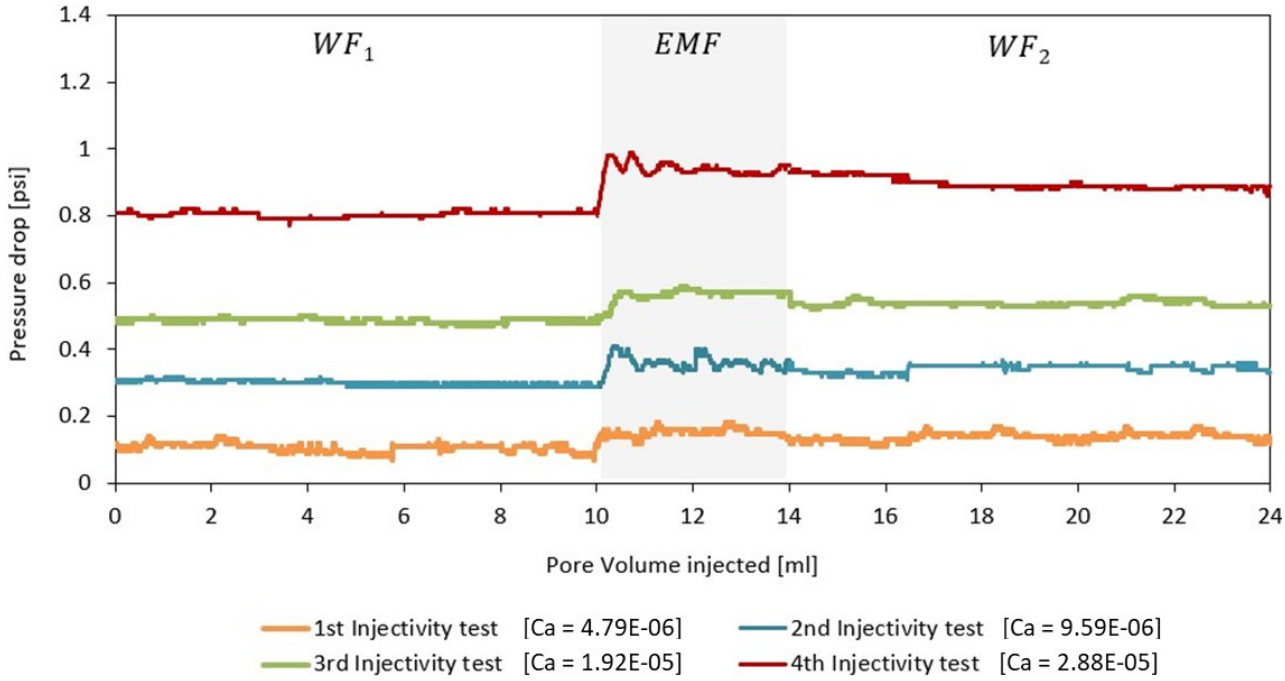

Figure 8. Differential pressure response during fluids injection versus pore volume injected in each injectivity test

of S_{or} since the objective was to carry out the test at a fixed Ca. This had a greater influence on the 3^{rd} test which, due to the very high flow rate, the S_{or} before WF_1 was lower around 23.60% of the micromodel P_v, and right after the injections EMF, and WF_2, the additional oil recovered was low.

The microscope processed images in Figures 9, 10, and 11 shows the phase distribution before and after the injection of just 1 P_v of emulsion. As can be seen, in all cases after WF_2 most of the oil droplets of the injected emulsion were trapped on the inlet face of the micromodel in the low permeability region. The droplets that passed through the region of high permeability at the lower Ca test ($2.39E{-}06$), percolated up to half of the micromodel in length. At the middle Ca test ($4.79E{-}06$) few droplets remained in the micromodel.

At the higher Ca test ($9.59E{-}06$), the droplets completely percolated through the micromodel, evidencing the influence of the Ca on the emulsion blockage and oil recovery. Comparing the injectivity and WAE tests at the same Ca, $4.79E{-}06$ for example, it is noted that the amount of droplets trapped in the high permeability region decreased significantly, explained by the change in the wettability due to the presence of residual oil films attached to the pore walls, facilitating the percolation of the droplets, making wettability a relevant parameter to be studied in future tests.

After emulsion flooding, the oil droplets blocked the water pathways, diverting the flow to the oil-containing pores during all tests. The differential pressure curves during the injections and the cumulative oil recovery curves in each WAE test are shown in Figure 12, with the WF_1, EMF, and WF_2 phases highlighted in the graph in relation to the injected P_v. The graph shows the pressure curves during WF_2, EMF, and WF_2. During the WF_1 stage, the device was completely saturated with oil and water in it S_{wi}. At this moment, the first pressure peak is expected since the viscosity ratio between oil and water is high, until it reaches the breakthrough and the pressure stabilizes. The second peak in the graph is due to emulsion injection, as a pressure gradient is created by droplets entrapment in the pore to divert the flow. Such behavior can be observed in all tests.

Table 2. WAE tests parameters

WAE test	Ca	S_{wi} (%)	S_{oi} (%)	S_{or} (%) **after WF_1**	S_{or} (%) **after WF_2**	**Trapped emulsion** [%]	-ΔS_{or} %
1^{st}	2.39 E-06	1.00	99.00	52.30	39.60	4.80	12.70
2^{nd}	4.79 E-06	0.40	99.60	54.30	30.20	1.20	24.10
3^{rd}	9.59 E-06	0.60	99.40	23.60	19.40	0.30	4.20

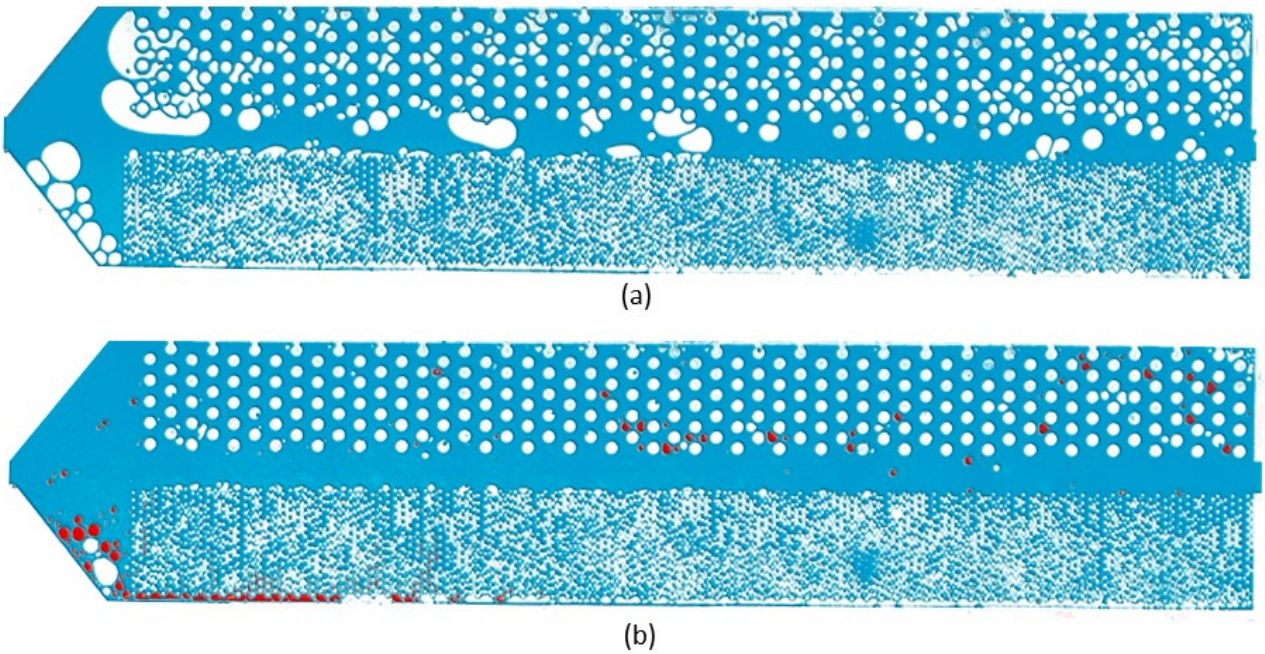

Figure 9. 2D X-Y cross section processed micromodel image of the 1^{st} WAE test ($Ca = 2.39E{-}06$) after (a) WF_1 and (b) WF_2. The oil phase and the background of the micromodel appear in white, the aqueous phase in blue and the emulsion droplets in red.

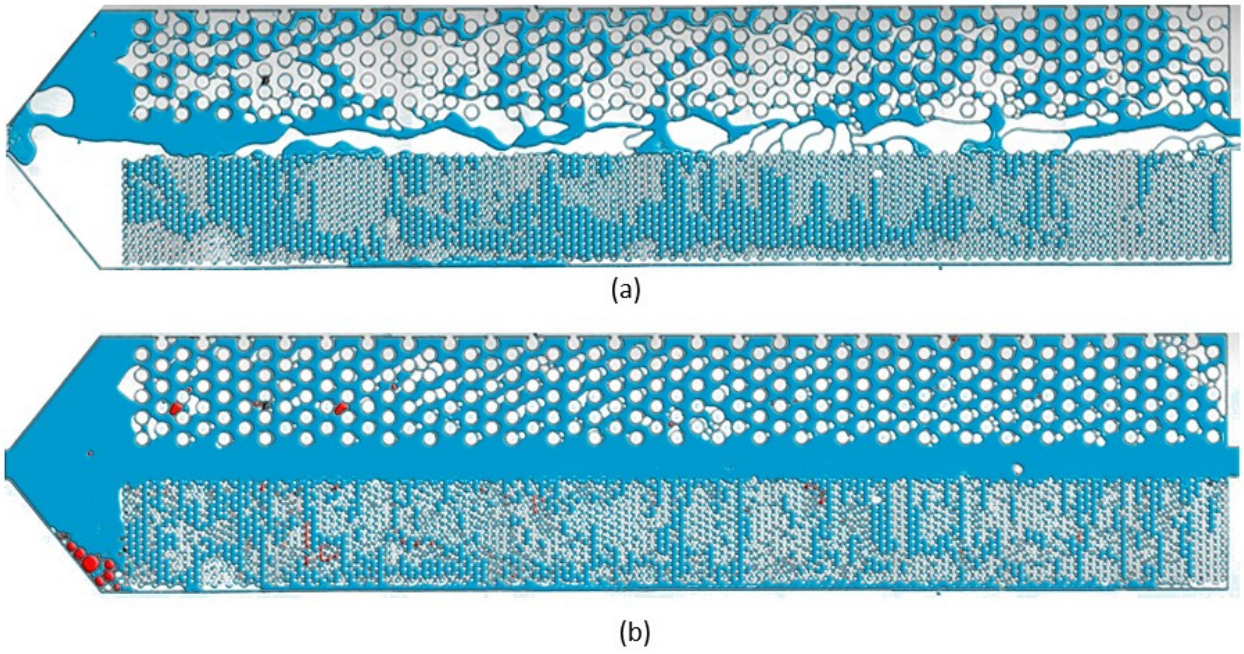

Figure 10. 2D X-Y cross section processed micromodel image of the 2^{nd} WAE test ($Ca = 4.79E{-}06$) after (a) WF_1 and (b) WF_2. The oil phase and the background of the micromodel appear in white, the aqueous phase in blue and the emulsion droplets in red.

4. CONCLUSIONS

This work aimed to experimentally investigate the flow of an O/W stable emulsion at pore scale in fractured microfluidic porous media. Emulsion stability of was analyzed through the evolution of drop size distribution (DSD) and bottle tests. Emulsion flow behavior was studied through emulsion flooding in a 2D Linear microfluidic device fabricated with Norland Optical Adhesive 81 (NOA), representing a porous media system with layered permeability, through injectivity and WAE tests at room temperature. During emulsion injection in single-phase flow, water

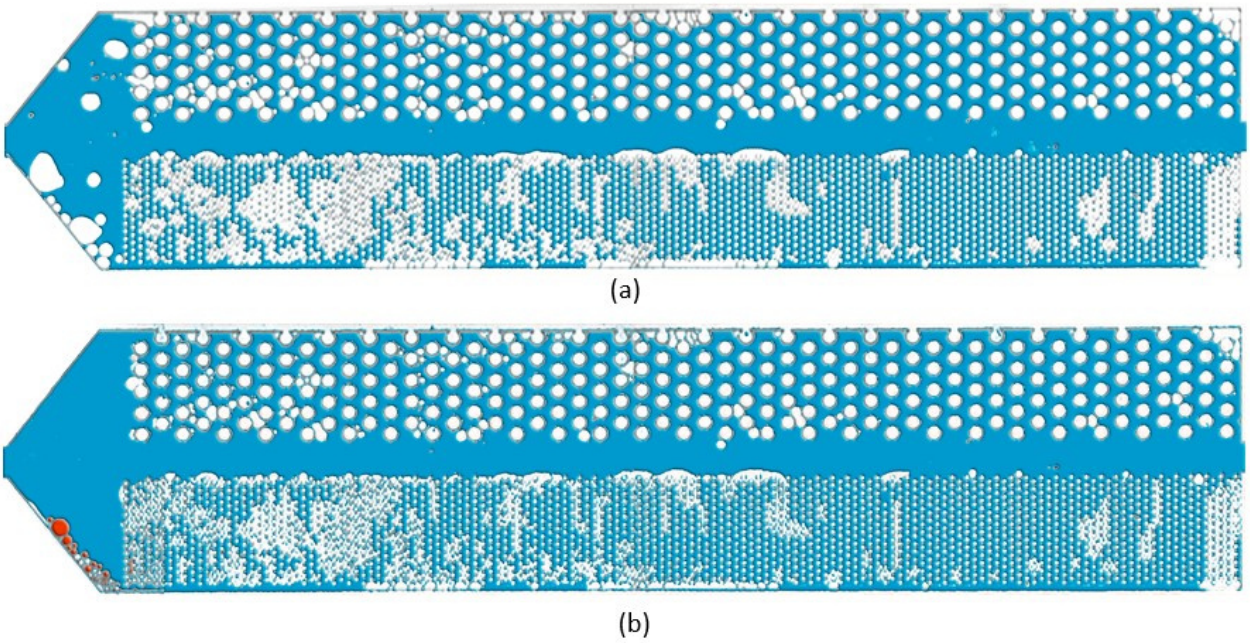

Figure 11. 2D X-Y cross section processed micromodel image of the 3^{rd} WAE test ($Ca = 9.59E{-}06$) after (a) WF_1 and (b) WF_2. The oil phase and the background of the micromodel appear in white, the aqueous phase in blue and the emulsion droplets in red.

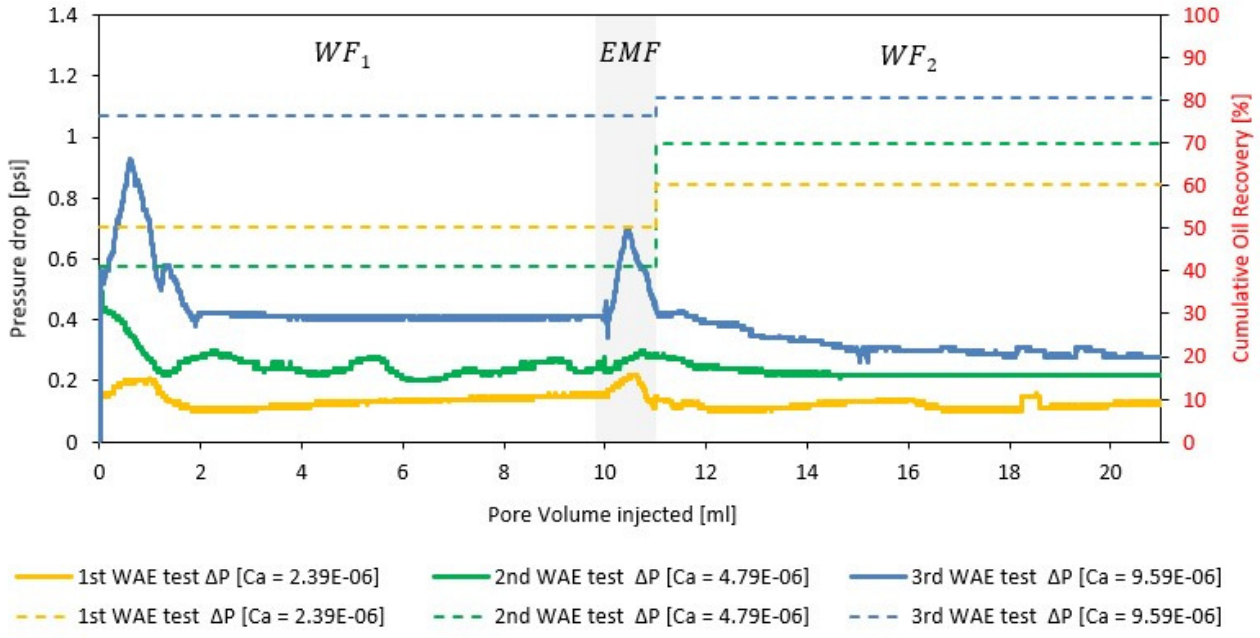

Figure 12. Differential pressure response during fluids injection and cumulative Oil Recovery curves for each fluids pore volume injected during oil displacement experiments

mobility control was observed through the reduction of the permeability to emulsion aqueous phase injection as a strong function of capillary number (Ca).

Though WAE test, influence of Ca in emulsion blockage effectiveness and in paraffin oil displacement mechanisms were observed. It was possible to show an increase in the oil volume recovered by WAE injection, proving a positive response to the technique in naturally fractured reservoirs. Despite the complexities, it was possible to obtain results similar to those in the literature in homogeneous porous media, working with adequate capillary number range and ideal emulsion/pore size ratio.

5. ACKNOWLEDGEMENTS

The authors acknowledge the Coordination for the Improvement of Higher Education Personnel (CAPES) for financial support.

6. REFERENCES

Allan, J. and Sun, S.Q., 2003. "Controls on recovery factor in fractured reservoirs: lessons learned from 100 fractured fields". In *SPE annual technical conference and exhibition*. OnePetro.

Alvarado, V., Garcia-Olvera, G., Hoyer, P., Lehmann, T.E. *et al.*, 2014. "Impact of polar components on crude oil-water interfacial film formation: A mechanisms for low-salinity waterflooding". In *SPE Annual Technical Conference and Exhibition*. Society of Petroleum Engineers.

Camargo, C., Vidal Vargas, J.A., Ruidiaz, E., Winter, A., Koroishi, E., Vidal Trevisan, O., Almeida, R. and Soares Bassani, G., 2019. "Study of the effect of low salinity water injection on the oil recovery factor in fractured carbonate rocks using computed tomography". In *offshore technology conference Brasil*. OnePetro.

Chen, G. and Tao, D., 2005. "An experimental study of stability of oil–water emulsion". *Fuel processing technology*, Vol. 86, No. 5, pp. 499–508.

Chen, Z., Dong, M., Husein, M. and Bryant, S., 2018. "Effects of oil viscosity on the plugging performance of oil-in-water emulsion in porous media". *Industrial & Engineering Chemistry Research*, Vol. 57, No. 21, pp. 7301–7309.

Cobos, S., Carvalho, M. and Alvarado, V., 2009. "Flow of oil–water emulsions through a constricted capillary". *International Journal of Multiphase Flow*, Vol. 35, No. 6, pp. 507–515.

Conn, C.A., Ma, K., Hirasaki, G.J. and Biswal, S.L., 2014. "Visualizing oil displacement with foam in a microfluidic device with permeability contrast". *Lab on a Chip*, Vol. 14, No. 20, pp. 3968–3977.

Guillen, V.R., Romero, M.I., da Silveira Carvalho, M. and Alvarado, V., 2012. "Capillary-driven mobility control in macro emulsion flow in porous media". *International Journal of multiphase flow*, Vol. 43, pp. 62–65.

Li, K. and Firoozabadi, A., 2000. "Experimental study of wettability alteration to preferential gas-wetting in porous media and its effects". *SPE Reservoir Evaluation & Engineering*, Vol. 3, No. 02, pp. 139–149.

Mandal, A., Samanta, A., Bera, A. and Ojha, K., 2010. "Characterization of oil- water emulsion and its use in enhanced oil recovery". *Industrial & engineering chemistry research*, Vol. 49, No. 24, pp. 12756–12761.

McAuliffe, C.D. *et al.*, 1973. "Oil-in-water emulsions and their flow properties in porous media". *Journal of petroleum technology*, Vol. 25, No. 06, pp. 727–733.

McDonald, J.C. and Whitesides, G.M., 2002. "Poly (dimethylsiloxane) as a material for fabricating microfluidic devices". *Accounts of chemical research*, Vol. 35, No. 7, pp. 491–499.

Vavra, E.D., Zeng, Y., Xiao, S., Hirasaki, G.J. and Biswal, S.L., 2018. "Microfluidic devices for characterizing pore-scale event processes in porous media for oil recovery applications". *JoVE (Journal of Visualized Experiments)*, , No. 131, p. e56592.

Wright, R., 1933. "Jamin effect in oil production". *AAPG Bulletin*, Vol. 17, No. 12, pp. 1521–1526.

Xia, Y. and Whitesides, G.M., 1998. "Soft lithography". *Annual review of materials science*, Vol. 28, No. 1, pp. 153–184.

Yu, L., Ding, B., Dong, M. and Jiang, Q., 2018. "Plugging ability of oil-in-water emulsions in porous media: experimental and modeling study". *Industrial & Engineering Chemistry Research*, Vol. 57, No. 43, pp. 14795–14808.

Zhou, Y., Yin, D., Chen, W., Liu, B. and Zhang, X., 2019. "A comprehensive review of emulsion and its field application for enhanced oil recovery". *Energy Science & Engineering*.

7. RESPONSIBILITY NOTICE

The authors are the only responsible for the printed material included in this paper.